CHAPTER-V

DYNAMICAL CONDUCTIVITY OF QUANTUM WIRE SYSTEM

In this chapter, we present a calculation of longitudinal and transverse macroscopic as well as microscopic dynamical conductivity for quantum wire system using formalism reported in chapter II. The macroscopic and microscopic longitudinal conductivity is computed to study conduction in different wave vector and frequency regime for quantum wire system in diffusive regime. The transverse polarizability cannot be defined for one dimensional system and it is found that quantum wire system does not support the propagation of transverse electric modes. The dynamical microscopic conductivity of quantum wire system is determined by both momentum and energy transfer processes. Screening of electric field due to electron-electron interaction takes place at finite value of momentum transfer along the direction of a wire. Plasmons in quantum wire system cannot be excited for negligibly small value of momentum transfer along x-direction

5.1   Introduction

Primary motivation in the study of semiconductor nanostructures have been to understand how the size of a semiconductor material influences its electronic properties. Interesting and size dependent spatial properties exist in these materials when their size is small as compared to the scale length of the election hole pair (the exciton Bohr-radius). In this limit, called as strong confined regime, the electron and hole wave functions experience 3D-quantum confinement due to the nanostructure boundary Quantum mechanical phase coherence (characteristics of microscopic objects) can be maintained over a distance of several microns in QWS. Elastic impurity scattering does not destroy the phase coherence and the effects of quantum interference can modify the properties. Quantum interference becomes more important when dimensionality is reduced The electron-electron interaction introduces a purely quantum mechanical correlation between the motion of electrons, which can result in a significant change in the properties of QWS at low temperature. The quantum size effects results from modulation of density of states in the channel of width compared to Fermi wavelength QWS have high mobility, large Fermi wavelength ($\lambda_F \sim 40$nm) comparable to size of wire, electron mean free path is quite large (exceedingly 10 μm)

The resistivity rises with the decrease in temperature in the low temperature regime, which is related to weak localization, can be quite pronounced in QWS. Long range correlation in diffusive motion of electrons is purely quantum mechanical interference corrections persists over phase coherence length. The quantum interference effect leads to a large change in several properties. Another important effect observed in QWS is weak localization. Weak localization is a quantum effect caused by the coherent back scattering, where an electron with initial momentum $\mathbf{k}$ is finally scattered into opposite state-$\mathbf{k}$ elastically. When weak localization is induced and controlled by potential structure, the efficiency of QWS device is enhanced. Localization process depends on the shape of potential and resulting electron states.

Interaction effects such as Coulomb blockade, single electron tunneling oscillations, Wigner-type crystallization etc. play a crucial role in the understanding of the electrical transport properties of QWS. Coulomb blockade resulting from energy change of the Coulomb oscillation for which electron-electron interaction plays an essential role. The suppression of tunneling between the peaks by Coulomb repulsion is known as Coulomb blockade. Many processes contribute to the electron relaxation (Coulomb interaction, impurity scattering, phonon emission etc.). In QWS, the LO phonons emission is most efficient one, while carrier-carrier Coulomb interaction is drastically reduced with respect to the bulk due to the reduced efficiency of carrier-carrier scattering. Semiconductor nanostructures make it possible to investigate the electron-phonon interaction beyond the bulk approximation. In this regime, strong quantum-size effects influence the electronic and vibrational states and their coupling. Other phenomena like quantum Hall effect, phase coherence length, conductance quantization, magnetic focussing, magnetotransport have been observed in QWS because of their interesting electrical transport characteristics due to their coherent ballistic electrons.

Collective electronic excitations in quantum wires has been observed by far infrared transmission spectroscopy [1-4] and resonant inelastic light scattering [5-7]. At low frequencies Q1D plasmons have been found, while at high frequencies, not only the 2D intersubband excitation, but charge density modes have been observed. These modes originate from a coupling of lateral and vertical electron motion. It has recently been proposed [8] that modulated Q1D systems might support current driven plasma instabilities at much lower threshold velocities than in 3D systems. The plasmon dispersion relation for the unmodulated case in closely linked [9,10] to the dimensionality and depends on the

width, but is insensitive to the geometry. It has been shown that, unlike the intersubband plasmon and electronic eigen energies, the intrasubband plasmon frequencies is only marginally dependent on the wire shape. Hwang and Das Sharma [11] have calculated the coupled plasmon-phonon modes in 1D GaAs based QWS in mean field approximation. They used the theory to obtain inelastic scattering rate of QW electrons as a function of their energy. They found that 1D plasmon phonon mode coupling effect is stronger than that in two and three dimension and mode coupling is stronger on 1D quantum wire at all electronic density in contrast to higher dimensions.

Citrin [12] found that intrinsic radiative lifetime of an axially symmetric GaAs/ GaAl$_{1-x}$As quantum wire is longer than radiative lifetime of a quantum well with comparable width because the lateral confinement in QWS imposes the decrease in excitonic coherence length. Zheng and Das Sarma [13] calculated Coulomb scattering lifetimes of electrons in two subband QWS within framework of RPA using dynamical dielectric function. They have found that the scattering rate of two subband QW is different from that of one subband QW. Liang [14] has studied the size effect on exciton-phonon scattering in QW. Electron mobility $\mu = e\tau/m^*$. is related to the relaxation time of the exciton-phonon scattering where m* is the exciton mass. At first τ decreases with decrease in well width. After reaching its maximum. τ increases as well width decreases further. Studies on electron scattering due to confined and extended acoustic phonons for Q1D quantum wire embedded within bulk AlAs [15] has shown that the deformation coupling between electrons and confined phonons is extremely small in comparison with that between electron and extended phonons. The scattering rate is found to decrease because of confined phonon emission. The most efficient energy relaxation process or excited electron gas in quantum wires is to emit LO phonons.

As the system size changes from larger than the electron phase coherence length to smaller than the elastic scattering length. the system goes through the universal conductance fluctuation region into ballistic transport region [16,17]. In the ballistic transport region quantization of conductance has been carried without an external magnetic field [18,19]. Numerical analysis of experimental results for ballistic electron wave propagation from a quantum point contact to a quantum wire have been reported [20]. It is found that transport characteristic of system depend on subject's shape. Numerical results show that for soft confinement, rounded corner model and magnetic field could suppress the oscillations. Using electron beam lithography, the high mobility (1×10^6 cm^2/vs) of 2 to 10μm long quantum

wire has been reported [21]. The quantized conductance in long wire is given by $2k_0e^2/\hbar$,[22] where k_0 is the correlation exponent that depends on the strength of the interaction. Transport through a clean 1D wire of [23], interacting electrons connected to semi infinite leads, is investigated. The d.c. conductance is found to be entirely determined by the properties of the leads. The influence of local defects on the d.c. transport in mesoscopic QWS of finite width has been investigated. From the results for the conductance and conductance fluctuations of narrow quantum wire with disorder, it is found that the conductance quantization is easily destroyed by strong scattering. Conductance fluctuations in narrow quantum wires are not universal (as in metallic regime) but can be independent of the wire length over a short range of lengths [24].

The aim of this chapter is to present a model calculation of dynamical macroscopic as well as microscopic conductivities of QWS using the formalism reported in chapter II. The macroscopic conductivity is computed to study the conduction in different wave vector and frequency regime, for QWS in diffusive regime. Our calculation are applied to GaAs/AlAs QWS Propagation of Plasmons and transverse electric (TE) modes is studied by calculating longitudinal and transverse microscopic conductivity, respectively. It is concluded that propagation of TE mode in QWS is not possible Modeling of QWS is given in sec. 5 2, whereas calculation of macroscopic and microscopic conductivity is reported in sec. 5.3. Results from our calculations are discussed in sec. 5 4 and finally we conclude our work in sec. 5.5

5.2   Modeling of QWS

For our theoretical calculation. we model QWS prepared from GaAs/$Al_xGa_{1-x}As$ structure as 1D sequence of quantum wires along with y-direction embedded into a host media of dielectric constant, ε_b. The quantum wires consist of a strong epitaxial confinement in z-direction on which a weak confinement is imposed in the perpendicular (x-direction). The confinement in z direction is much stronger than the confinement in y direction. In terms of energy scales the energy level separation is about few meV in y direction, while in z direction it is of the order of 0.01 eV. In the low regimes if the 2D electron density is not to high ($n_s < 5 \times 10^{11}$ cm^{-2}) we can assume that electrons are always in the lowest subband in z direction. Delta function type confinement is assumed along z-axis. The confining potential within a quantum wire is assumed to be of infinite potential type. A free particle motion for an electron is assumed along x-direction with effective mass, m_x^* and tight binding wave

function along y axis. Tight binding part of the wave function consists of envelope functions which vary over width of wire along y-axis.

The single particle wave function and energy eigen values for QWS are given by

$$\phi_k(r) = \exp(ik_x x) \sum_{k_y} \phi_{jk_y}(y) \, \phi(z) \tag{5.1}$$

and

$$E_k = \hbar^2 k_x/2m_x^* + E_j, \tag{5.2}$$

where $\phi_{jk_y}(y)$ corresponds to electron motion along y-axis in jth subband. $\phi(z)$ represents the confinement along z-axis. Wave function $\phi(z)$ is strongly confined within thin layer, we take $|\phi(z)|^2 \rightarrow \delta(z)$. k_x and k_y are components of wave vector in x-and-y directions, respectively. E_j represents the energy levels (mini-bands) along y-axis. The single particle wave function comprises of free electron wave function for motion along x axis and tight binding wave function along y-axis. Tight binding part of wave function consists of envelope function which vary over width of wire along y axis. We confine ourselves to quantum limit and take $\phi_{jk_y}(y)$ in following form

$$\phi_{jk_y}(y) = \sum_{n} \exp(ik_y nd) \, U_j(y-nd), \tag{5.3}$$

where n is the wire index and d is the length of the unit cell along y-direction. The $U_j(y-nd)$ is an envelope function confined to jth subband in nth wire. For modeling a quantum wire as an infinite potential well of width (a) along y-axis. $U_0(y)$ can be taken of following form

$$U_0(y) = (2/a)^{1/2} \sin[\pi(y/a + 1/2)]. \tag{5.4}$$

In following we consider intrasubband transitions (j=0).

5.3   Formalism and calculations

Motion of electrons in QWS is essentially restricted to 1D and QWS exhibit Q1D electronic properties We first consider the case of macroscopic conductivity of QWS

5.31 Macroscopic conductivity

As is reported in chapter II, the 2D macroscopic conductivity is given by

$$\sigma^{L/T}(\rho,\rho',\omega) = -(i\omega e^2/2\pi) \int \ln|\rho-\rho''| \, \alpha^{L/T}(\rho'',\rho',\omega) \, d^2\rho'', \quad (5.5)$$

where $\rho=(x,y)$ is 2D vector. On performing continuous Fourier transformation along x-axis, which is considered as the direction of motion of electron, Eq.(5.5) reduces to

$$\sigma^{L/T}(q_x,y,y',\omega) = -(i\omega e^2/2q_x)\int exp(-iq_x|y-y''|)\alpha^{L/T}(q_x,y'',y',\omega) \, dy''. \quad (5.6)$$

q_x is the wave vector along x-direction. As was mentioned before, electrons are mainly confined to their respective wire (non-tunnelling). Equation (5.6) can be rewritten in terms of wire indices in the following forms

$$\sigma^L(q_x,l,l',\omega) = -(i\omega e^2/2q_x) \iint \alpha_e^L(q_x,\omega) \, exp(-iq_x|(l-l')d+y-y'|)$$
$$|U_0(y)|^2 |U_0(y')|^2 dy \, dy', \quad (5.7)$$

where use of $\alpha_e^L(q_x,l,l',\omega)=\alpha_e^L(q_x,\omega)\delta_{ll'}$ has been made. Suffix T has been dropped in Eq.(5.7) because of the fact that $\alpha_e^L(q_x,\omega)$ cannot be defined for a 1D system. Electric field and wave vector cannot be perpendicular to each other in a 1D system. With the use of following discrete Fourier transform

$$f(q_x,q_y,\omega) = \sum_{ll'} f(q_x,l,l',\omega)exp[-iq_y(l-l')d] \quad (5.8)$$

we get

$$\sigma^L(q_x,q_y,\omega)=[(\gamma-i\omega)e^2/2q_x]\alpha_e^L(q_x,\omega)U(q_x,q_y)-(i\omega/4\pi)(\varepsilon_b-1), \quad (5.9)$$

where

$$U(q_x,q_y) = H(q_x)-C(q_x) \, [1-S(q_x,q_y)] \quad (5.10)$$

and

$$S(q_x,q_y) = sinh(q_x d)/[cosh(q_x d)-cos(q_y d)]. \quad (5.11)$$

The structure factors $H(q_x)$ and $C(q_x)$ are obtained from Eq.(3.17) and (3.18) on replacing q by q_x and L by a. The q_y takes discrete values due to confinement of electron motion within a quantum wire along y-axis, whereas q_x is a continuous variable. At zero temperature, $\alpha_e^L(q_x,\omega)$ is given by [25]

$$\alpha_e^L(q_x,\omega)=(m_x^*/\pi q_x)\ \ln\{[\omega(\omega+i\gamma)-(E_{q_x}-q_xv_F)^2]/[\omega(\omega+i\gamma)-(E_{q_x}+q_xv_F)^2]\},$$

$$(5.12)$$

where $E_{q_x}=\hbar^2q_x^2/2m_x^*$ and $v_F=\pi n_1\hbar/2m_x^*$ is 1D Fermi velocity, n_1 is number of electrons per unit length. For the case of $q_x\ll \pi n_1/2$ (Fermi wave vector in 1D) and $q_xv_F\ll|\omega+i\gamma|$, Eq.(5.12) reduces to

$$\alpha_{1D}^L(q_x,\omega) = - [n_1q_x^2/ m_x^*\omega(\omega+i\gamma)].$$

$$(5.13)$$

For d→0, Eq.(5.9) with the use of Eq.(5.13), gives 2D dynamical conductivity. By taking q_x→0 and q_y=0, we obtain long wavelength 1D conductivity which is given by

$$\sigma_{1D}(\omega) = [n_1e^2/ m_x^*(\gamma-i\omega)],$$

$$(5.14)$$

which is the Drude formula of 1D conductivity. As longitudinal and transverse parts of conductivity are equal in long wavelength limit, Eq.(5.14) can also be used to describe $\sigma_{1D}^T(\omega)$ which is independent of q_x.

5.32 Microscopic conductivity

The longitudinal and transverse microscopic conductivity of QWS are obtained from Eqs.(2.18) and (2.29) by taking δ-function type confinement along z-axis. We Fourier transform Eqs.(2.18) and (2.29) with respect to x and then take δ-function type confinement along z-axis. We obtain

$$\tilde{\sigma}^L(q_x,y,y',\omega) = \sigma^L(q_x,y,y',\omega) - \iint\alpha^L(q_x,y,y_1,\omega)V(q_x,y_1,y_2)$$

$$\tilde{\sigma}^L(q_x,y_2,y',\omega)dy_1\,dy_2 \qquad (5.15)$$

and

$$\tilde{\sigma}^T(q_x,y,y',\omega) = \sigma^T(q_x,y,y',\omega) + (i\omega/c^2) \iint \tilde{\sigma}^T(q_x,y,y_1,\omega)$$

$$G(q_x,y_1,y_2,\omega)\sigma^T(q_x,y_2,y',\omega)dy_1\,dy_2, \qquad (5.16)$$

where

$$V(q_x,y,y') = 2e^2\,k_0(|q_x(y-y')|) \qquad (5.17)$$

and

$$G(q_x,y,y',\omega) = 2k_0(|p_x(y-y')|) \qquad (5.18)$$

with

$$p_x = (q_x^2 - \omega^2/c^2)^{1/2}. \qquad (5.19)$$

$k_0(|q_x(y-y')|)$ is the zeroth order modified Bessel function, which diverges as $-\ln|q_x(y-y')|$ when q_x goes to zero. Further, Eqs.(5.15) and (5.16) can be written in terms of wire indices l and l' in following form:

$$\tilde{\sigma}^L(q_x,l,l',\omega) = \sigma^L(q_x,l,l',\omega) - 2\,\alpha^L(q_x,\omega) \sum_{l''} \iint dy\,dy'\tilde{\sigma}^L(q_x,l,l'',\omega)$$

$$|U_0(y-l''d)|\,k_0(|q_x(y-y')|)|U_0(y'-l'd)| \qquad (5.20)$$

and

$$\tilde{\sigma}^T(q_x,l,l',\omega) = \sigma^T(q_x,l,l',\omega) + (2i\omega/c^2) \sum_{l''} \int dy \int dy'\tilde{\sigma}^T(q_x,l,l'',\omega)$$

$$|U_0(y-l''d)|k_0(|p_x(y-y')|)|U_0(y'-l'd)|. \qquad (5.21)$$

With the use of discrete Fourier transform with respect to l and l', Eqs.(5.20) and (5.21) reduces to

$$\tilde{\sigma}^L(q_x,q_y,\omega) = \sigma^L(q_x,q_y,\omega)-\alpha^L(q_x,\omega)V(q_x,q_y)\tilde{\sigma}^L(q_x,q_y,\omega) \qquad (5.22)$$

and

$$\tilde{\sigma}^T(q_x,q_y,\omega) = \sigma^T(q_x,q_y,\omega) + \sigma^T(q_x,q_y,\omega)G(q_x,q_y,\omega)\tilde{\sigma}^T(q_x,q_y,\omega),$$

$$(5.23)$$

103

where

$$V(q_x,q_y) = 2e^2 \sum_{l\text{-}l'} \iint k_0(|q_x(l\text{-}l')d+y\text{-}y'|) \exp[-iq_y(l\text{-}l')d] \, |U_0(y)|^2$$
$$U_0(y')|^2 \, dy \, dy' \qquad (5.24)$$

and

$$G(q_x,q_y,\omega) = (2i\omega/c^2) \sum_{l\text{-}l'} \iint k_0(|p_x(l\text{-}l')d+y\text{-}y'|) \exp[-iq_y(l\text{-}l')d]$$
$$|U_0(y)|^2 \, U_0(y')|^2 \, dy \, dy'. \qquad (5.25)$$

Equations (5.22) and (5.23) can be transformed to

$$\tilde{\sigma}_{QW}^L(q_x,q_y,\omega) = \sigma_{QW}^L(q_x,q_y,\omega) \, / \, \varepsilon_{QW}(q_x,q_y,\omega) \qquad (5.26)$$

and

$$\tilde{\sigma}_{QW}^T(q_x,q_y,\omega) = \sigma_{QW}^T(q_x,q_y,\omega) \, / \, F_{QW}(q_x,q_y,\omega), \qquad (5.27)$$

where

$$\varepsilon_{QW}(q_x,q_y,\omega) = \varepsilon_b + \alpha_e^L(q_x,\omega)V(q_x,q_y) \qquad (5.28)$$

and

$$F_{QW}(q_x,q_y,\omega) = 1 - \sigma_{QW}^T(q_x,q_y,\omega) \, G(q_x,q_y,\omega). \qquad (5.29)$$

Equation (5.24) and (5.25) can be simplified by first carrying out summation over l and l' and then performing integration over y and y' The Bessel function $k_0(q_x|y\text{-}y'|)$ can be represented in several ways. Li and Das Sarma evaluated $V(q_x,q_y)$, using periodic boundary condition along y-axis by assigning finite size to QWS [25] However, their results do not yield correct limiting value for d→0 and d→∞. One of the form of $k_0(q_x|y\text{-}y'|)$ which correctly reproduces 2D results for d→0 is

$$k_0(q_x|y\text{-}y'|) = \int_0^\infty dt \, \exp(-|y\text{-}y'|\sqrt{t^2+q_x^2}) \, / \, \sqrt{t^2+q_x^2}. \qquad (5.30)$$

We solve Eq.(5.24) using (5.30) to get

$$V(q_x,q_y) = 2e^2 \int_0^\infty dt \, U(\lambda_x,q_y) \, /\lambda_x, \qquad (5.31)$$

where

$$\lambda_x = \sqrt{t^2+q_x^2} \qquad (5.32)$$

and

$$U(\lambda_x, q_y) = H(\lambda_x) - C(\lambda_x) [1 - S(\lambda_x, q_y)].$$ (5.33)

$U(\lambda_x, q_y)$ and $S(\lambda_x, q_y)$ are obtained from Eqs.(5.10) and (5.11), respectively on replacing λ_x by q_x. For the case of $d\rightarrow 0$, $H(\lambda_x) \cong C(\lambda_x) \cong 1$ and $S(\lambda_x, q_y) \cong 2\lambda_x/(\lambda_x^2 + q_y^2)d$, which on substituting into Eq.(5.31) yields

$$V(q_x, q_y) = 2\pi e^2/qd,$$ (5.34)

where $q = q_x^2 + q_y^2$. Substitution of Eq.(5.13) and (5.34) in (5.28) gives correct value of 2D dielectric function for the case of $q_y=0$ and $qd<<1$. Similarly, $G(q_x, q_y, \omega)$ is obtained from Eq.(5.25), using Eq.(5.30)

$$G(q_x, q_y, \omega) = (2i\omega/c^2) \int_0^\infty dt\, U(\lambda_x', q_y) /\lambda_x',$$ (5.35)

where

$$\lambda_x' = \sqrt{t^2 + p_x^2}.$$ (5.36)

For $d\rightarrow 0$, $G(q_x, q_y, \omega)$ is given by

$$G(q_x, q_y, \omega) = 2\pi i\omega/pc^2 d.$$ (5.37)

On substituting Eqs.(5.37) and (5.14), we get

$$F(q_x, \omega) = 1 + 2\pi(n_1/d)e^2/m_x'pc^2.$$ (5.38)

$F(q_x, \omega)$ given in Eq.(5 38) can never go to zero for any value of q_x and ω. This suggests that transverse electric modes cannot propagate in a 2D system of charge carriers [26]. This argument can be extended to conclude that TE modes can also propagate in a Q2D system or QWS. right hand side of Eq.(5.29) can never be zero. In next section, we discuss our results on macroscopic as well as microscopic longitudinal dynamical conductivity. To evaluate microscopic longitudinal conductivity for an arbitrary value of d, we use method suggested by Li and Das Sarma [25] to calculate $V(q_x, q_y)$. With the use of periodic boundary condition along y-direction by assigning finite size (L) to QWS along y-axis. $V(q_x, q_y)$ is given by [25]

$$V(q_x, q_y) = (2e^2/d)\int dy \int dy' \, |U_0(y)|^2 S(q, y-y') |U_0(y')|^2$$ (5.39)

with

$$S(\mathbf{q},y-y')=\sum_{l}\exp[-i(q_y+2\pi l/d)(y-y')]/[q_x^2+(q_y+2\pi l/d)^2]^{1/2}, \quad (5.40)$$

where l is an integer. Equation (5.40) can be simplified with the use of envelope function for ground subband i.e. Eq.(5.4) to obtain

$$V(q_x,q_y) = (64\pi^4 e^2/d) \sum_{l} [1-\cos(q_y a+2\pi la/d)] / (q_y a+2\pi la/d)^2 \times$$

$$(a/d)/[4\pi^2-(q_y a+2\pi la/d)^2]^2[(q_x a)^2+(q_y a+2\pi la/d)^2]^2. \quad (5.41)$$

The generalized dielectric function of QWS can be obtained from Eq.(5.28) by using Eqs.(5.12) and (5.41). The collective excitation spectrum of QWS are studied by solving $\varepsilon_{QW}(q_x,q_y,\omega)=0$. The microscopic conductivity of QWS is given by Eq.(5.26) by making use of Eq.(5.28) and (5.9).

5.4 Results and discussion

Our main results on dynamical conductivity of QWS are given by Eqs.(5.9) and (5.26). We have computed the real part of $\sigma_{QW}(q_x,q_y,\omega)$ and $\tilde{\sigma}_{QW}(q_x,q_y,\omega)$, as real part of them correspond to physically measurable quantities. For computation of our results we model GaAs/Al$_x$Ga$_{1-x}$As QWS in terms of following values of parameters: m_x^*=0.068 m_e, d=78 nm. a=39 nm, ε_b=12.5 and n_1=0.872x10^6 cm^{-2} As is shown in previous section. Eq.(5.9) reduces to Drude formula of 1D conductivity, Eq.(5.14). for $q_x d\ll1$. $q_y d\rightarrow 0$ and $q_x v_F\ll|\omega+i\gamma|$. For ω=0, Eq.(5.14) gives

$$\sigma_{1D} = (n_1 e^2 / dm_x^*\gamma). \quad (5.42)$$

We plot our computed $Re\sigma_{QW}(q_x,q_y,\omega)$, real part of $\sigma_{QW}(q_x,q_y,\omega)$ as a function of ω in Fig. 5.1 for different combinations of $q_x d$ and $q_y d$ values (i) $q_x d$=0.01 and $q_y d$=0.001, (ii) $q_x d$=0.1 and $q_y d$=0.001 and (iii) $q_x d$=0.1 and $q_y d$=0 1. As expected the behaviour of $Re\sigma_{QW}(q_x,q_y,\omega)/\sigma_{1D}$ for first case is similar to that of $(\gamma^2 /\gamma^2+\omega^2)$. For $\gamma\gg\omega$ and $\omega\rightarrow 0$, $Re\sigma_{QW}(q_x,q_y,\omega)$ reduces to Drude conductivity, whereas for $\omega^2\gg\gamma^2$, $Re\sigma_{QW}(q_x,q_y,\omega)$ shows $1/\omega^2$ dependence. For case (ii) and (iii), $Re\sigma_{QW}(q_x,q_y,\omega)$ shows a peak which

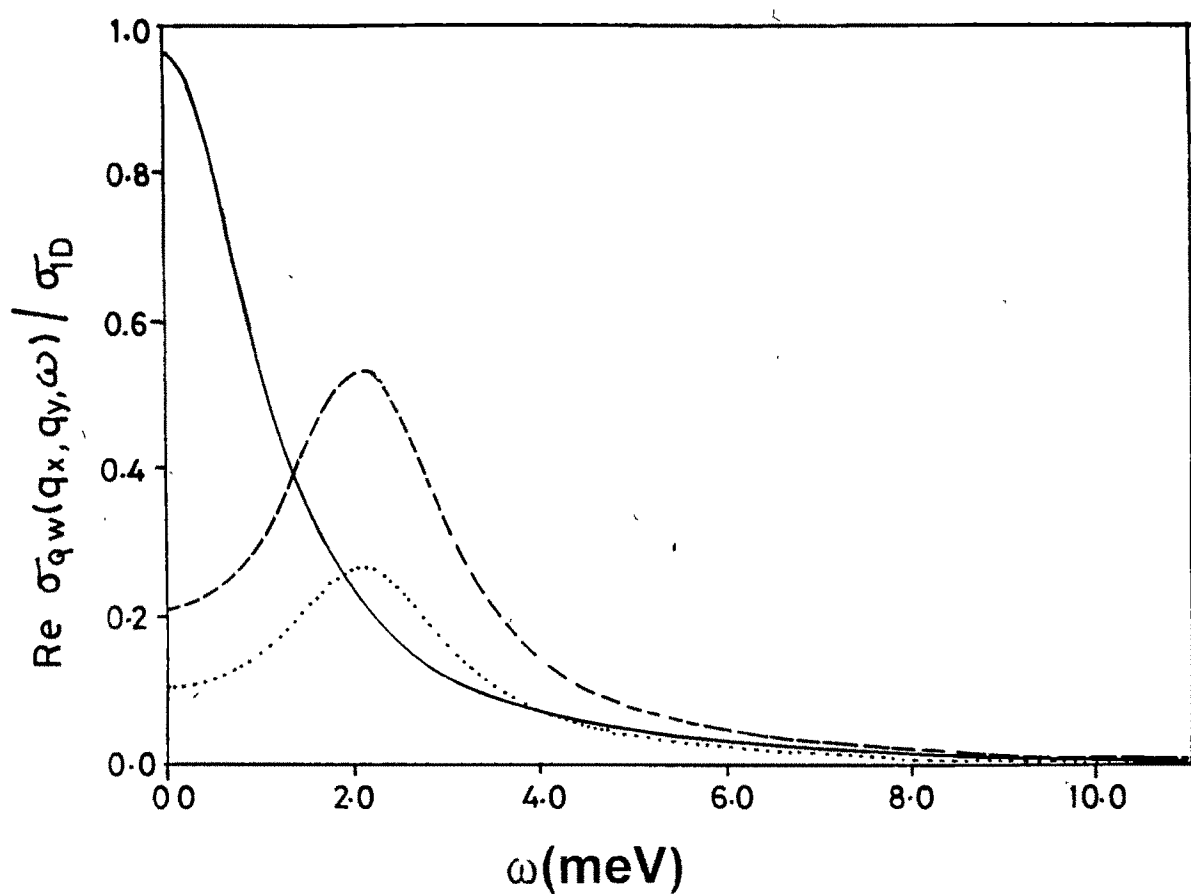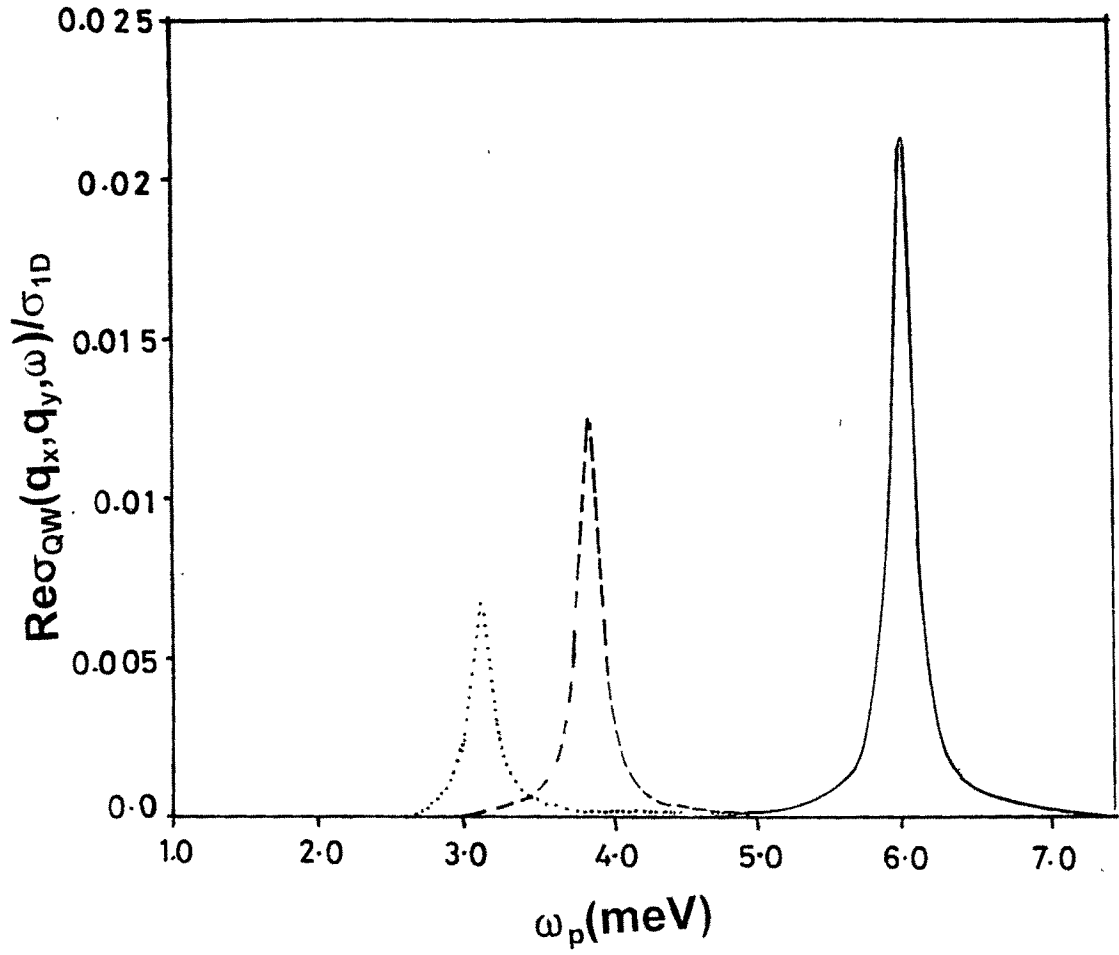**Fig. 5.1** Plot of $\mathrm{Re}\sigma_{QW}(q_x,q_y,\omega)/\sigma_{1D}$ versus ω for $q_xd=0.01$ & $q_yd=0.001$ (full curve), $q_xd=0.1$ & $q_yd=0.001$ (dash-dash curve) and $q_xd=0.1$ & $q_yd=0.1$ (dot-dot curve).

Fig. 5.2 The $Re\tilde{\sigma}_{QW}(q_x, q_v, \omega)/\sigma_{1D}$ is plotted as a function of ω for $q_x d=1.0$ & $q_y d=\pi$ (dot-dot curve), $q_x d=1.0$ & $q_y d=\pi/2$ (dash-dash curve) and $q_x d=2.0$ & $q_y d=\pi$ (solid line curve).

corresponds to single particle excitations. As is seen from figure, the position of peak shifts toward higher ω-values, peak height decreases and half width of peak increases on increasing $q_x d$ at given $q_y d$-value. Peak position, half width of peak and height of peak represent frequency, inverse of single particle scattering time and amplitude of excitation, respectively of single particle excitation mode excited by longitudinal component of field, at given value of q_x and q_y. On increasing wave vector (q_x or q_y) single particle excitation peak becomes broader and small, suggesting that these excitation can disappear for very large value of q_x and q_y ($q_x d \gg 1$ and $q_y d \gg 1$). It is found that peak position is independent of q_y, whereas peak height reduces and half width of peak increases on increasing q_y. The q_x-dependence of peak height and half width has been found to be weaker in case of $\cos(q_y d)=1$, as compared with that for $\cos(q_y d)=-1$.

Our computed $\text{Re}\tilde{\sigma}_{QW}(q_x,q_y,\omega)/\sigma_{1D}$ is plotted as a function of ω for (i) $q_x d=1.0$, $q_y d= \pi$ (ii) $q_x d=1.0$, $q_y d=\pi/2$ and (iii) $q_x d=2.0$ and $q_y d=\pi$ in Fig. 5.2. $\text{Re}\tilde{\sigma}_{QW}(q_x,q_y,\omega)$ shows a well defined symmetric peak which corresponds plasma oscillations (collective excitations) in QWS. We notice that if $q_x d$ is kept fixed the peak height reduces and peak position shift towards higher ω-values on changing $\cos(q_y d)$ from -1 to 1. Under the case of single particle excitations, half width of peak in $\text{Re}\tilde{\sigma}_{QW}(q_x,q_y,\omega)$ is independent of q_x and q_y. This is because of independence of γ, which determines the half width of peak in $\text{Re}\sigma_{QW}(q_x,q_y,\omega)$, on changing q_x and q_y. Figure also suggests that maximum conductivity is achieved along the wire, where $q_y d \to 0$. at all values of $q_x d$.

The behaviour of height of peak in $\text{Re}\tilde{\sigma}_{QW}(q_x,q_y,\omega)$ versus ω for fixed $q_x d$-values on changing $q_y d$ has been found similar to that of Re $\sigma_{QW}(q_x,q_y,\omega)$, except that the peak position of $\text{Re}\tilde{\sigma}_{QW}(q_x,q_y,\omega)$ depend more strongly on $q_y d$. We notice that $\text{Re}\sigma_{QW}(q_x,q_y,\omega) \ll \text{Re}\sigma_{QW}(q_x,q_y,\omega)$ because of screening effects which are incorporated in $\text{Re}\tilde{\sigma}_{QW}(q_x,q_y,\omega)$. To learn more about peak position which corresponds to plasma frequency, we solved $\varepsilon_{QW}(q_x,q_y,\omega)=0$ for ω as a function of q_x and q_y. Solution of

$$\varepsilon_b + \alpha_\varepsilon^L(q_x,\omega)V(q_x,q_y) = 0 \qquad (5.43)$$

gives

$$\omega_P(q_x,q_y) = \{[A(q_x,q_y)\omega_+^2-\omega_-^2]/[A(q_x,q_y)-1]\}^{1/2}, \qquad (5.44)$$

where
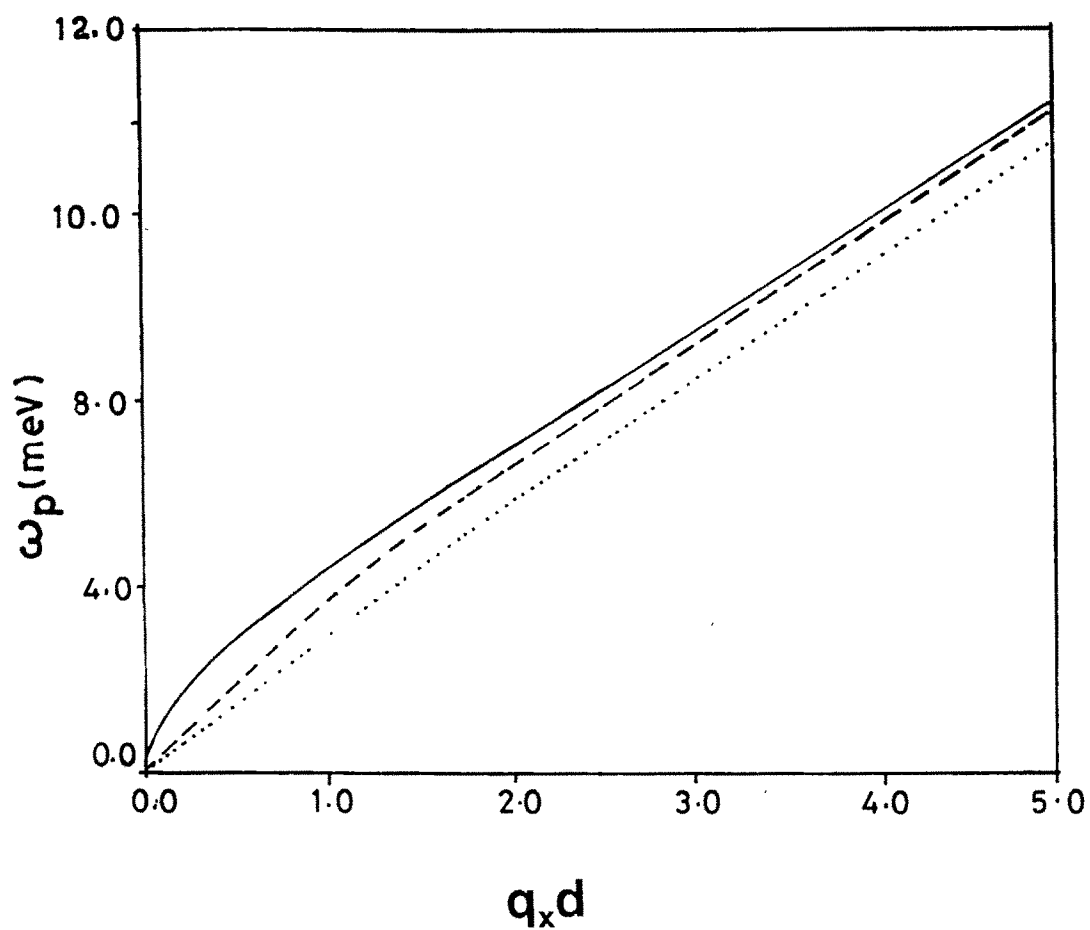
Fig. 5.3   The intrasubband plasmons of QWS as a function of $q_x d$

for three values of $q_y d$: $\cos(q_y d)=1$ (solid line curve). $\cos(q_y d)=0$

(dashed curve) and $\cos(q_y d)= -1$ (dotted curve)

$$A(q_x,q_y) = \exp[\pi q_x/m_x^* V(q_x,q_y)] \tag{5.45}$$

and

$$\omega_\pm = [q_x v_F \pm q_x^2/2m_x^*]. \tag{5.46}$$

In long wavelength limit ($q_x \to 0$ and $q_y \to 0$). Eq.(5.46) goes to

$$\omega_P \sim q_x a\, \omega_0| \ln(q_x a)|^{1/2}, \tag{5.47}$$

where

$$\omega_0 = (2n_1 e^2/m_x^* a^2)^{1/2}. \tag{5.48}$$

Computed $\omega_P(q_x,q_y)$ as a function of $q_x d$ for $-1 \leq \cos(q_y d) \leq 1$ is plotted in Fig. 5.3. It is interesting to note that, unlike the case of a superlattice, $\omega_P(q_x,q_y)$ goes to zero for all values of $\cos(q_y d)$ when $q_x d \to 0$. Also, the width of band of $\omega_P(q_x,q_y)$ is smaller as compared to that 2D plasmon band of a superlattice. Similarity between the band of $\omega_P(q_x,q_y)$ (which consists of 1D plasmons) and the band of 2D plasmons of a superlattice is that the upper and lower edge of $\omega_P(q_x,q_y)$ occur at $\cos(q_y d)=1$ and $\cos(q_y d)=-1$, respectively, where upper and lower edge plasmon band of superlattice appear at $\cos(q_z d)=1$ and $\cos(q_z d)=-1$, respectively. However, for $q_x d \to 0$. $\varepsilon_{QW}(q_x,q_y,\omega)$ goes to ε_b, which suggests screening of field diminishes and plasmons cannot be excited in a QWS for negligibly small momentum transfer along the direction of a quantum wire.

We next discuss our results for static case ($\omega \to 0$) of $\mathrm{Re}\sigma_{QW}(q_x,q_y,\omega)$, for different values of $q_y d$ (0. 0 01. 0 1) $\mathrm{Re}\sigma_{QW}(q_x)$ reduces to σ_{1D} for $q_x \to 0$ and $q_y=0$ Looking at Fig. 5.4 we find that behaviour of $\mathrm{Re}\sigma_{QW}(q_x,q_y)$ with $q_x d$ for given value of $q_y d$ is similar to that $\mathrm{Re}\sigma_{QW}(q_x,q_y)$ versus ω at fixed $q_x d$. $\mathrm{Re}\sigma_{QW}(q_x,q_y)$ shows a peak when $q_x d$ and $q_y d$ are roughly equal. The peak become smaller and broader on increasing $q_y d$. This suggests that momentum transfer which is represented by q_x and q_y and energy transfer coming through ω play equally important role in determination of $\mathrm{Re}\sigma_{QW}(q_x,q_y,\omega)$. Therefore, to determine correct dynamical conductivity, one must allow all momentum transfer processes to take place. Negligibly small value of $\mathrm{Re}\sigma_{QW}(q_x,q_y)$ for $q_x d \to 0$ at non-zero value of $q_y d$ suggests that current mainly flows along the direction of the wire of QWS, for finite momentum transfer. We further find that $\mathrm{Re}\tilde{\sigma}_{QW}(q_x,q_y) \ll \mathrm{Re}\sigma_{QW}(q_x,q_y)$ for $q_x d$ not close to zero and $\mathrm{Re}\tilde{\sigma}_{QW}(q_x,q_y) \sim \mathrm{Re}\sigma_{QW}(q_x,q_y)$ when $q_x \to 0$ because of disappearance of screening effects for $q_x d \to 0$.
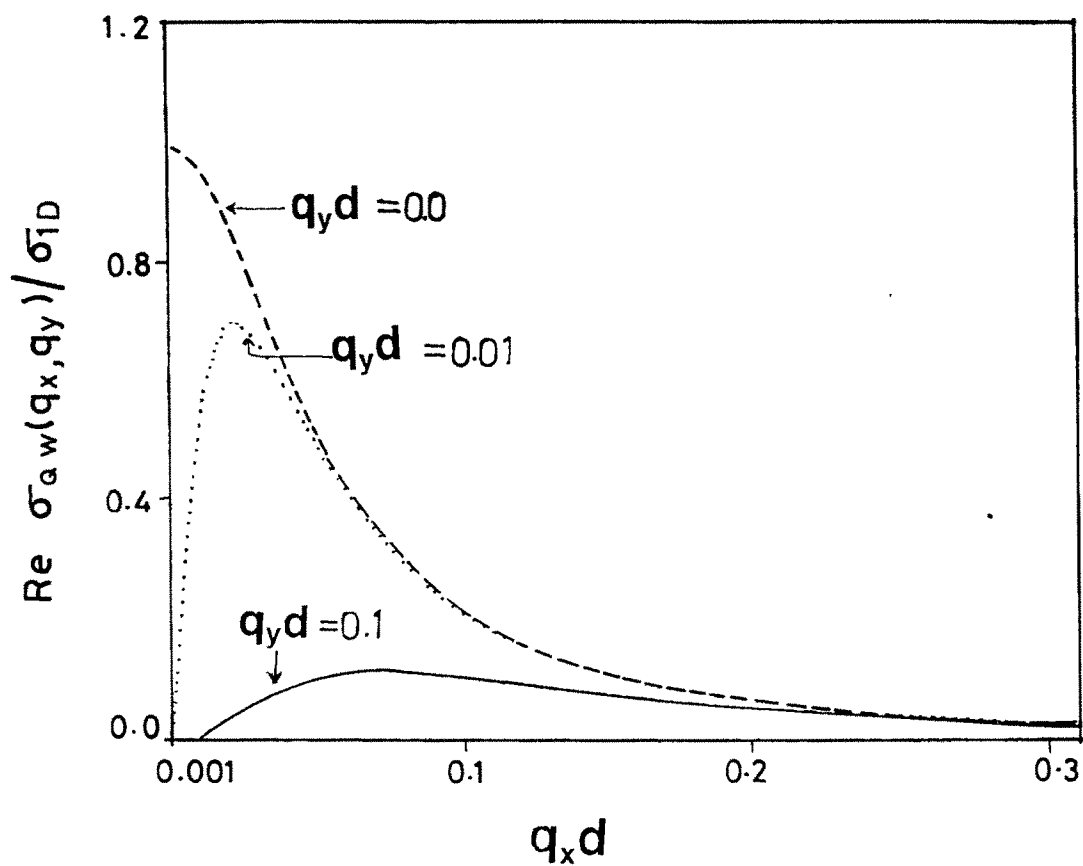
Fig. 5.4 The $\mathrm{Re}\sigma_{QW}(q_x,q_y)/\sigma_{1D}$ is plotted as a function of $q_x d$ for three values of $q_y d$.
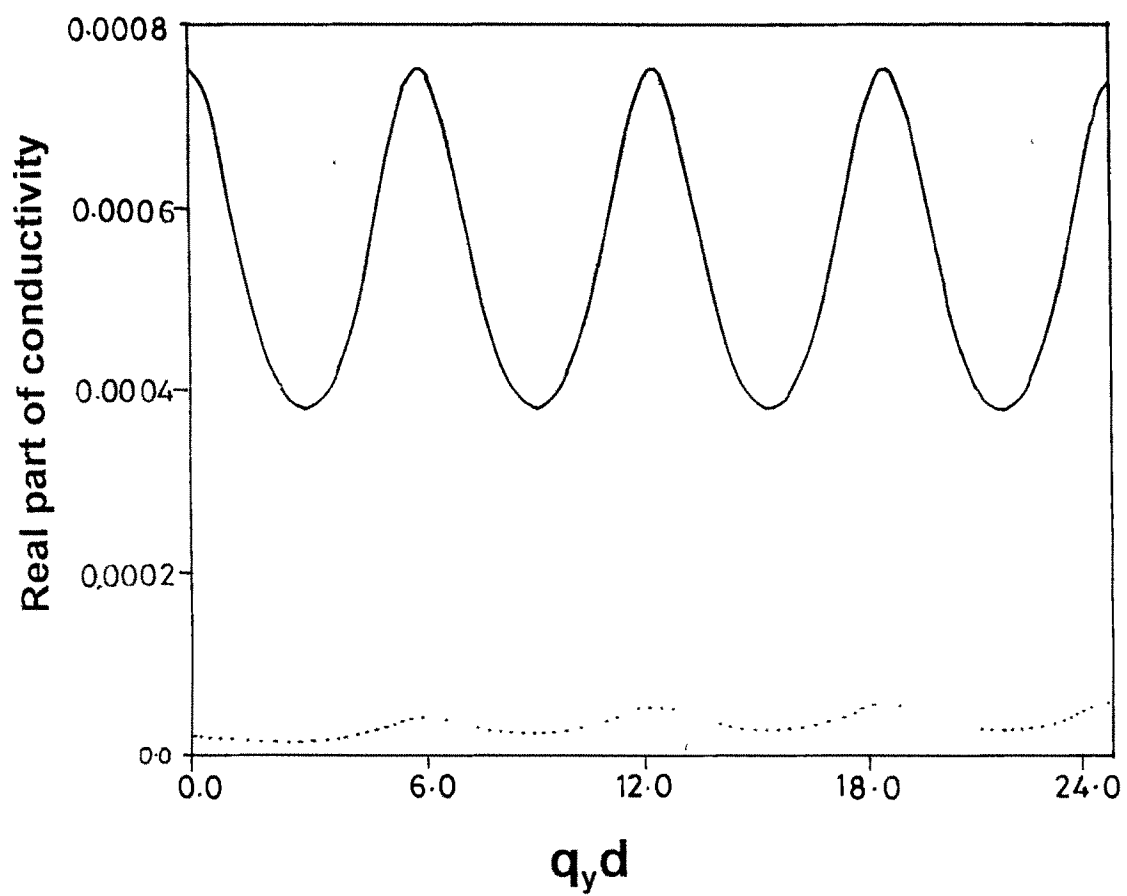
Fig. 5.5 A plot of $Re\sigma_{QW}(q_x,q_y)/\sigma_{1D}$ (full curve) and $Re\tilde{\sigma}_{QW}(q_x,q_y)/\sigma_{1D}$ (dotted curve) versus $q_y d$ for $q_x d = 2.0$

Figure 5.5 exhibits the computed $Re\sigma_{QW}(q_x,q_y)$ and $Re\tilde{\sigma}_{QW}(q_x,q_y)$ as a function of $q_y d$ for $\gamma=0.1$ meV, $q_x d=2.0$ and $n_1=0.872\times10^6$ cm^{-2}. Both $Re\sigma_{QW}(q_x,q_y)$ and $Re\tilde{\sigma}_{QW}(q_x,q_y)$ show oscillatory behaviour on increasing $q_y d$, which is characteristic of periodic structure of QWS along y-axis. The oscillations in $Re\sigma_{QW}(q_x,q_y)$ are greatly smoothened out suggesting that screening effect not only reduces the magnitude of longitudinal conductivity but also weakens q_y dependence of it. Our results, presented in this chapter, lacks the comparison with experimental results. So far our knowledge goes, no experimental results on wave vector dynamical conductivity exist in literature.

5.5 Conclusion

A calculation of $Re\sigma_{QW}(q_x,q_y,\omega)$ and $Re\tilde{\sigma}_{QW}(q_x,q_y,\omega)$ has been performed using the formalism given in chapter II. It is shown that $\alpha_e^T(q_x,\omega)$ cannot be defined for QWS and TE mode cannot propagate in QWS. Expressions for $Re\sigma_{QW}(q_x,q_y,\omega)$ and $Re\tilde{\sigma}_{QW}(q_x,q_y,\omega)$ which are valid for all values of q_x, q_y and ω are obtained. Our analysis of $Re\sigma_{QW}(q_x,q_y,\omega)$ suggests that both momentum transfer and energy transfer play equally important role in determining the dynamical macroscopic conductivity of QWS. It is also found that screening of electric field due to electron-electron interaction disappears for negligibly small value of momentum transfer along a direction of a quantum wire ($q_x d\rightarrow0$). However, for $q_x d$ not close to zero. $Re\tilde{\sigma}_{QW}(q_x,q_y,\omega)<< Re\sigma_{QW}(q_x,q_y,\omega)$ for all values of q_x, q_y and ω Unlike the case of a superlattice, plasmons cannot be excited in a QWS for $q_x d\rightarrow0$. for any value of $q_y d$

REFERENCES

[1]   W. Hansen, M. Horst, J.P. Kotthaus, U. Merkt, Ch. Sikorski and K. Ploog, Phys. Rev. Lett. 58, 2586 (1987).

[2]   F. Brinkop, W. Hanken, J.P. Kotthaus and K. Ploog, Phys. Rev. B 37, 6547 (1988).

[3]   T. Dermal. D Heitmann, P. Grambow and K. Ploog, Phys. Rev. B 38, 12372 (1988); Phys. Rev Lett. 66, 2657 (1991).

[4]   H. Drexler, W Hansen, J. Kotthaus, M. Holland and S.P. Beaumont, Phys. Rev. B 46, 12849 (1992).

[5]   J.S. Wannier, G. Danen, A. Pinczuk, J. Valladares, L.N. Pfeiffer and K.W. West, Phys. Rev. Lett. 63, 1641 (1989).

[6]   T. Egler, G. Abstreiter, G. Weigmann, T. Demel, D. Heitmann, P. Grambow and W. Schlapp, Phys. Rev. Lett. 65, 1884 (1990).

[7]   A.R. Goni, A. Pinczuk, J.S. Weiner. J.S. Calleja, B.S. Dennis, L.N. Pfeiffer and K.W. West, Phys. Rev. Lett. 67, 3298 (1991).

[8]   K. Kempa. P Bakshi and X. Xie. Phys. Rev B 48. 9153 (1993).

[9]   B.S. Mendoza and W.L. Schaich, Phys. Rev. B 43, 9275 (1991)

[10] B.S. Mendoza and Marcelo del Castillo-Mussot, Rev. Mex. Fis. 39, 640 (1993)

[11] S. Das Sarma and E.H. Hwang, Phys. Rev. B 54, 1936 (1996).

[12] P.H. Citrin, Phys. Rev. B 54, R11050 (1996).

[13] L. Zheng and S Das Sarma. Phys Rev B 53. 9964, (1996).

[14] S.D. Liang, C.Y. Chen. S C Liang and D.L. Lin, Phys. Rev B 53. 15459 (1996).

[15] N. Nishiguchi. Phys. Rev. B 54. 11494 (1996).

[16] S. He and S Das Sarma, Phys. Rev B 40. 3379 (1989).

[17] P.A. Lee. A.D. Stone and H. Fukuyama, Phys. Rev B 35, 1039 (1987).

[18] B.J. Van Wees et al, Phys. Rev. Lett. 60, 848 (1988).

[19] D.A. Wharam et al., J. Phys C 21, 1209 (1988).

[20] M. Saito, M. Takatsu, R.A. Kichl , N. Yokoyama and T. Usaki, Phys. Rev. B 52, 8224 (1995)

[21] T. Honda, S. Tarucha, T. Saku and Y. Tokura. Phys. Rev. B 53, 16403 (1996).

[22] Y. Takagaki, Y Tokura and S. Tarucha, Phys. Rev B 53, 15462 (1996).

[23] I. Safi and H.J. Schulz, Phys. Rev B 52, 17040 (1995).

[24] Y. Tokura and S. Tarucha. Phys. Rev B 53 16403 (1996).

[25] Q.P. Li and S Das Sarma. Phys. Rev. B 43, 11768 (1991).

[26] H. Shi and A. Griffin, Phys Rev. B 44, 11977 (1991).